

Shadows and photon rings of a spherically accreting Kehagias-Sfetsos black hole

Mohaddese Heydari-Fard^{1*}, Malihe Heydari-Fard^{2†} and Nematollah Riazi^{1‡}

¹ *Department of Physics, Shahid Beheshti University, Evin 19839, Tehran, Iran*

² *Department of Physics, The University of Qom, 3716146611, Qom, Iran*

July 6, 2023

Abstract

By considering Kehagias-Sfetsos black hole in the framework of the Hořava-Lifshitz gravity, we study the optical appearance of such black holes surrounded by spherical accretion flow. For the static/infalling spherical accretion flow, we compute the observed specific intensity as a function of impact parameter. We also investigate the effect of the Hořava parameter and accreting matter on the luminosity of shadows and photon rings. It is found that an increase in the Hořava parameter decreases the shadow size, while the shadows and photon rings luminosities increase. Moreover, we constrain the Hořava parameter from the observational data reported by the Event Horizon Telescope for M87* and Sgr A*.

Keywords: Black hole shadow, Spherical accretion, Modified theories of gravity

1 Introduction

The Event Horizon Telescope (EHT) collaboration released the first image of a black hole shadow [1]–[7]. The image is formed by null geodesics in the strong gravity regime. The photons with large energy fall into the black hole and form a dark area for a distant observer, while photons with small energy coming from infinity will be pushed back by the gravitational potential of the black hole. However, the photons with critical energy will revolve around the black hole an infinite time and surround the dark interior, which are called the photon ring and the black hole shadow, respectively. In a seminal work, Synge calculated the angular radius of the shadow of Schwarzschild black hole [8]. Then, Bardeen studied the shadow of Kerr black hole and argued that the angular momentum cause the deformation of its shadow [9].

By modelling M87* with the Kerr geometry in general relativity (GR), the observation was found to be in agreement with the predictions of GR. However, due to the EHT systematic uncertainties it is still possible to test the alternative theories of gravity by simulating the black hole image and observing deviations from the Kerr solution. To this end, one can explore the distortion in the black hole image which contains valuable information about the structure of space-time around a black hole solution. This motivated many authors over the recent years to study the black hole shadow in the context of modified theories of gravity [10]–[21].

On the other hand, the astrophysical black holes are expected to be surrounded by sources of the luminous accretion material which makes it possible to investigate how the observational appearance of the black hole from the accretion flow. Indeed, before the discovery of the black hole shadow by EHT, the possible observational characteristics of the black hole shadow by considering different accretion flows were studied. Luminet was the

*Electronic address: m_heydarifard@sbu.ac.ir

†Electronic address: heydarifard@qom.ac.ir

‡Electronic address: n_riazi@sbu.ac.ir

first to investigate the optical properties of the Schwarzschild black hole in 1979, and constructed the simulated shadow image of the Schwarzschild black hole surrounded by an emitting thin accretion disk [22]. The simulated image obtain by Luninet is remarkably similar to the black hole shadow image captured by EHT [1]. He found that the emergence of the shadow and ring depends on the position and profile of the accretion flow and the inner edge of disk can have a remarkable signature in the image. Thereafter, Falcke et al. by considering the radiation of a hot optically thin accretion flow around a supermassive black hole in the center of our galaxy created a ray-tracing code to obtain the images of Sgr A*, and showed that the black hole shadow is equivalent to the gravitational lensing effect [23]. For a geometrically thick and optically thin accretion disk, the gravitational lensing and the shadow of the Schwarzschild black hole was studied by Cunha et al. [24]. Gralla et al. by considering the Schwarzschild black hole with both thin and thick accretion disks, investigated the trajectory of light rays and ring that surrounds the black hole shadow. It was found that the shadow size depends on the position of the accretion disk as well as the emission profile of the model [25]. However, when the Schwarzschild black hole is surrounded by spherically symmetric accretion flow, Narayan et al. showed that the location of the outer edge of the shadow is independent of the inner radius at which the accreting gas stops radiating [26]. Therefore, the size of the shadow depends on the space-time geometry and does not affected by the details of the accretion flow. Also, the optical appearance of black holes surrounded by various accretions in modified gravity theories, have been extensively studied [27]–[47].

Amongst the many modifications of GR that have been suggested is the Hořava-Lifshitz gravity which is motivated by the need to include the quantum effects in the low-mass limit. The theory is a renormalizable four-dimensional theory of gravity which reduces to the Einstein’s gravity with non-vanishing cosmological constant in the IR limit but with improved UV behaviors. A class of static and spherically symmetric black hole solutions of the theory with a cosmological constant was obtained in [48]. Among them, the Ads type solution has an asymptotic behavior differs from the Schwarzschild-Ads solution in GR; namely in the IR limit the theory of GR is not always recovered. However, in the context of the modified Hořava model, a static spherically symmetric solution with asymptotically flat behavior, which is a counterpart of the Schwarzschild black hole in GR, has been obtained by Kehagia and Sfetsos [49]. This solution usually known as the KS black hole. Then, in the slow rotation approximation, the black hole solution in the IR regime has been obtained in [50]–[51]. In literatures, many physical aspects of KS black hole have already been studied [52]–[63]. Moreover, for cosmological implications of Hořava-Lifshitz gravity see for instance Refs.[64]–[76].

The shadows and rings of the KS black hole surrounded by thin accretion disk have been studied in [77]. However, the optical appearance of the KS black hole surrounded by spherical accretion flow has not yet been studied. So, in the present work, we consider the KS black hole surrounded with static/infalling accretion flows and discuss the effects of Hořava parameter and spherical accretion on the observed appearance of the black hole.

The paper is organized as follows. In section 2, after a brief review of KS black holes, we discuss the photon trajectories in the space-time of such black holes and investigate the effects of the Hořava parameter on them. Then we present the shadow images of KS black hole with static and infalling spherical accretion flows in section 3 and section 4, respectively. The paper ends with concluding remarks in section 5.

2 KS black holes and trajectory of surrounding photons

A. KS geometry

In the ADM formalism of Hořava-Lifshitz gravity the four-dimensional metric is parameterized as [64]

$$ds^2 = -N^2 c^2 dt^2 + g_{ij}(dx^i + N^i dt)(dx^j + N^j dt), \quad (1)$$

where N , N_i and g_{ij} are the lapse function, the shift function and three-dimensional spatial metric, respectively.

The action of the IR-modified Hořava gravity is

$$\mathcal{S} = \int dt dx^3 \sqrt{g} N \left[\frac{2}{\kappa^2} (K_{ij} K^{ij} - \lambda K^2) - \frac{\kappa^2}{2\nu^4} C_{ij} C^{ij} + \frac{\kappa^2 \mu}{2\nu^2} \epsilon^{ijk} R_{il}^{(3)} \nabla_j R_k^{(3)l} \right]$$

$$- \left[\frac{\kappa^2 \mu^2}{8} R_{ij}^{(3)} R^{(3)ij} + \frac{\kappa^2 \mu^2}{8(3\lambda - 1)} \left(\frac{4\lambda - 1}{4} (R^{(3)})^2 - \Lambda_W R^{(3)} + 3\Lambda_W^2 \right) + \frac{\kappa^2 \mu^2 \tilde{\omega}}{8(3\lambda - 1)} R^{(3)} \right] \quad (2)$$

where $\mu, \nu, \lambda, \kappa, \tilde{\omega}$ and Λ_W are constant parameters. $R^{(3)}$ is the three-dimensional curvature scalar for g_{ij} and the extrinsic curvature, K_{ij} , is given by

$$K_{ij} = \frac{1}{2N} (\dot{g}_{ij} - \nabla_i N_j - \nabla_j N_i), \quad (3)$$

where the dot represents a derivative with respect to t and ∇_i denotes the covariant derivative with respect to the spatial metric g_{ij} . C^{ij} is the Cotton tensor, reads as

$$C^{ij} = \epsilon^{ikl} \nabla_k \left(R_l^{(3)j} - \frac{1}{4} R^{(3)} \delta_l^j \right). \quad (4)$$

Now, we consider the static and spherically symmetric metric as

$$ds^2 = -g_{tt}(r)dt^2 + g_{rr}(r)dr^2 + r^2 d\theta^2 + r^2 \sin^2 \theta d\varphi^2, \quad (5)$$

where $g_{tt}(r)$ and $g_{rr}(r)$ are functions of radial coordinate r . In the specific case of $\lambda = 1$, which reduces to the Einstein-Hilbert action in IR limit, the solution of the vacuum field equations can be obtained as follows

$$-g_{tt}(r) = 1/g_{rr}(r) = f(r) = 1 + (\tilde{\omega} - \Lambda_W)r^2 - \sqrt{r[\tilde{\omega}(\tilde{\omega} - 2\Lambda_W)r^3 + \beta]}, \quad (6)$$

with β is an integration constant. By considering $\beta = 4\tilde{\omega}M$ and $\Lambda_W = 0$ the KS asymptotically flat solution is given by [49]

$$f(r) = 1 + \tilde{\omega}r^2 \left[1 - \left(1 + \frac{4M}{\tilde{\omega}r^3} \right)^{1/2} \right], \quad (7)$$

with the M is the mass of the black hole and $\tilde{\omega}$ is the Hořava-Lifshitz parameter. By rearranging the parameter $\tilde{\omega}$ as $\tilde{\omega} = \frac{1}{2\omega^2}$, one can rewrite the metric function in the following form [77]

$$f(r) = 1 + \frac{r^2}{2\omega^2} \left(1 - \sqrt{1 + \frac{8M\omega^2}{r^3}} \right). \quad (8)$$

The radius of the outer and inner horizons can be found by solving $f(r) = 0$

$$r_{\pm} = M[1 \pm \sqrt{1 - \omega^2/M^2}]. \quad (9)$$

As is clear, for the existence of black hole solution a constraint $\omega/M \leq 1$ should be imposed and an extremal black hole, $r_+ = r_-$, corresponds to the case $\omega/M = 1$. Also, in the limit of $\omega \rightarrow 0$ the above metric becomes the static solution in GR which is described by the Schwarzschild metric. Note the parameter ω always takes the positive values. Thus, for the range $0 < \omega < 1$, the behavior of the inner horizon r_- and the event horizon r_+ , is plotted in the left panel of Fig. 1. The points at the beginning of each curve denote the corresponding values to the Schwarzschild solution.

B. Null trajectory around KS black hole

The trajectory of null geodesics in the space-time of KS black hole can be obtained using the Euler-Lagrange equations. Without loss of generality, we restrict ourselves to the equatorial panel, $\theta = \frac{\pi}{2}$. There are two constants of motion correspond to the energy E and angular momentum L of photons and the equations of motion are given by

$$\dot{t} = \frac{E}{f(r)}, \quad (10)$$

$$\dot{\varphi} = \frac{L}{r^2}, \quad (11)$$

$$\dot{r}^2 = E^2 - V_{\text{eff}}(r), \quad (12)$$

where the effective potential is as follows

$$V_{\text{eff}}(r) = \frac{L^2}{r^2} f(r) = \frac{L^2}{r^2} \left[1 + \frac{r^2}{2\omega^2} \left(1 - \sqrt{1 + \frac{8M\omega^2}{r^3}} \right) \right]. \quad (13)$$

We have displayed the effective potential for different values of the Hořava parameter, ω , in the right panel of Fig. 1. As one can see, the peak of the potential increases with increase of ω . Note that for non-radial geodesics, it is convenient to set $L = 1$ and thus we plot the figure for this value of the angular momentum.

Next, we focus on the photon motion in the vicinity of KS black hole. Combining equations (11) and (12) the differential equation governing the light rays trajectory can be obtained as

$$\left(\frac{dr}{d\varphi} \right)^2 = \frac{r^4}{b^2} - r^2 f(r) \quad (14)$$

where the impact parameter is defined as $b \equiv \frac{L}{E}$. In particular, for the photons with critical value of the impact parameter, $b = b_{\text{ph}}$, an unstable circular orbit occurs at the maxima of the effective potential at $r = r_{\text{ph}}$, known as the photon sphere [78]. To study circular orbits with constant radius $r = r_{\text{ph}}$ from equation (12) we have

$$V_{\text{eff}}(r_{\text{ph}}) = E_{\text{ph}}^2, \quad V'_{\text{eff}}(r_{\text{ph}}) = 0, \quad (15)$$

where prime denotes differentiation with respect to the radial coordinate r . Use of equation (13) leads to the following relation

$$r f'(r) - 2f(r) = 0 \quad (16)$$

which gives the radius of unstable photon circular orbits as

$$r_{\text{ph}} = 2\sqrt{3}M \cos \left[\frac{1}{3} \cos^{-1} \left(\frac{-4\omega^2}{3\sqrt{3}M^2} \right) \right]. \quad (17)$$

The dependence of the radius of the photon sphere r_{ph} on the parameter ω is also plotted in the right panel of Fig. 1, showing that r_{ph} is a decreasing function of the Hořava parameter. Moreover, we see that in the limiting case $\omega \rightarrow 0$, $r_{\text{ph}} = 3M$ which is the radius of the unstable circular photon orbit for the Schwarzschild black hole. The impact parameter of the photon sphere is also given by

$$b_{\text{ph}} = \frac{r_{\text{ph}}}{\sqrt{f(r_{\text{ph}})}} = \left(\frac{1}{r_{\text{ph}}^2} + \frac{1 - \sqrt{1 + \frac{8M\omega^2}{r_{\text{ph}}^3}}}{2\omega^2} \right)^{-\frac{1}{2}}, \quad (18)$$

which for an asymptotically flat space-time with a metric in the form (5) is equal to the radius of the black hole shadow. The results of the radii of the event horizon r_+ , photon sphere r_{ph} as well as the impact parameter of the photon sphere b_{ph} are also presented in Table. 1.

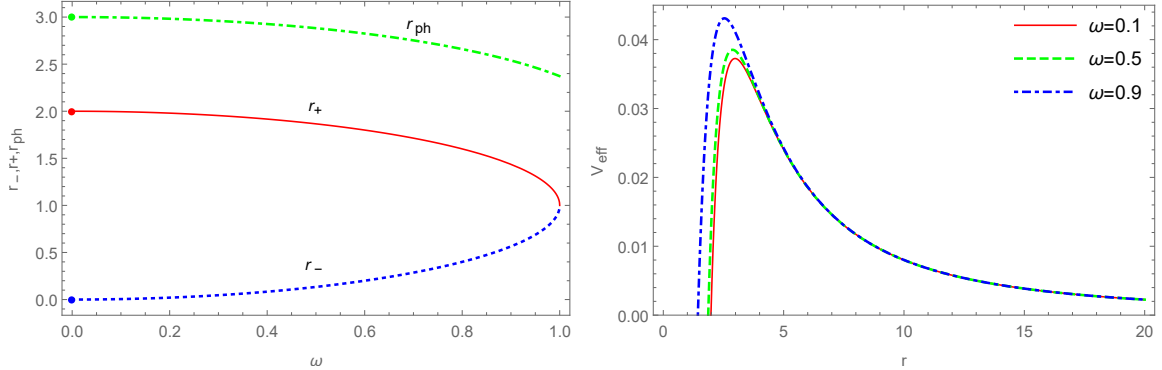


Figure 1: Left panel: The photon radii r_{ph} , r_- and r_+ as a function of Hořava parameter for $M = 1$. Right panel: The effective potential V_{eff} as a function of radius for different values of Hořava parameter.

Table 1: The values of the event horizon radius r_+ , photon radius, r_{ph} and impact parameter, b_{ph} for different values of ω . The first column with $\omega \rightarrow 0$ corresponds to the Schwarzschild black hole.

	$\omega \rightarrow 0$	$\omega = 0.1$	$\omega = 0.3$	$\omega = 0.5$	$\omega = 0.7$	$\omega = 0.9$
r_{ph}/M	3	2.9956	2.9592	2.8820	2.7524	2.5393
b_{ph}/M	5.1962	5.1923	5.1609	5.0951	4.9868	4.9117
r_+/M	2	1.9949	1.9539	1.8660	1.7141	1.4359
r_-/M	0	0.0050	0.0461	0.1339	0.2859	0.5641

From equation (14), it is clear that the trajectory of light rays depends on the impact parameter b . The photons with small angular momentum, $b < b_{\text{ph}}$, finally enter the black hole singularity, while photons with large angular momentum, $b > b_{\text{ph}}$, will be deflected and pushed back to the distant observer. For critical values of impact parameter $b = b_{\text{ph}}$, the photons swirl around the black hole on the photon sphere, with an infinite time. These photon trajectories are shown with green, gray and red curves in Fig. 2, respectively. The black disk also shows the event horizon surface. We have plotted the light trajectories for $\omega = 0.1$ and $\omega = 0.9$. As one can see, the event horizon radius and the radius of the photon sphere are smaller for a larger ω . This is because the larger values of ω weakens the strength of gravity so that the instability area around KS black hole decreases and thus the photon radius takes smaller values.

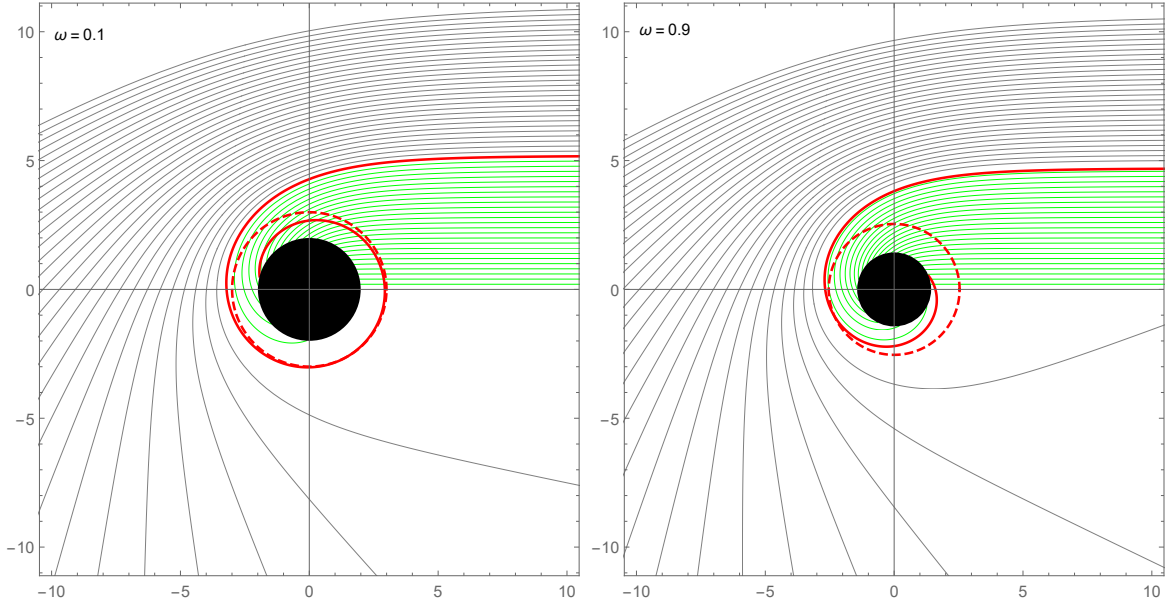


Figure 2: The trajectory of light rays around a KS black hole with $\omega = 0.1$ (left panel) and $\omega = 0.9$ (right panel). The red, gray and green curves correspond to the trajectory of light rays with $b = b_{\text{ph}}$, $b > b_{\text{ph}}$ and $b < b_{\text{ph}}$, respectively.

Now, we aim to investigate the constraints on the Hořava parameter using the EHT observations of the shadow of M87* and Sgr A*. As one can see from equation (18), the shadow size is dependent on the Hořava parameter and thus from EHT observational data we can impose bounds on it. For a distant observer, the angular diameter Ω of the black hole shadow is given by [79]

$$\Omega = \frac{2b_{\text{ph}}}{D}, \quad (19)$$

where D is the distance between the black hole and distant observer, and b_{ph} is obtained from equation (18). The above equation can be rewritten as

$$\left(\frac{\Omega}{\mu\text{as}} \right) = \left(\frac{6.191165 \times 10^{-8}}{\pi} \frac{\gamma}{D/\text{Mpc}} \right) \left(\frac{b_{\text{ph}}}{M} \right), \quad (20)$$

with γ is the mass ratio of the black hole to the Sun. From the reports released by EHT for the shadow of M87* the distance and mass correspond to $D = 16.8$ Mpc and $\gamma = 6.2 \times 10^9$, while for the shadow of Sgr A* these values are given by $D = 8.127$ kpc and $\gamma = 4.14 \times 10^6$, respectively [1]–[7]. In Fig. 3, we have plotted the diameter of the shadow of KS black hole as a function of Hořava parameter, using the data of M87* (red curve) and of Sgr A* (black curve). It is found that the Ω decreases with increase of ω . The cyan and yellow regions are also the shadow diameters of M87* and Sgr A* reported by the EHT observations. As we observe, the KS black hole is able to describe the shadow size of Sgr A*, provided that the Hořava parameter is constrained to the values in range $0 < \omega < 0.7766$, while the present data of M87* can not constrain the KS geometry.

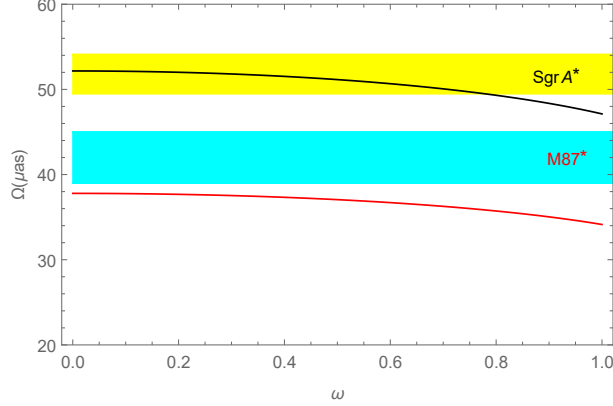


Figure 3: Shadow diameter of the KS black hole as a function of Hořava parameter, ω . The yellow and cyan regions are the experimental data of Sgr A* ($51.8 \pm 2.3 \mu\text{as}$) and M87* ($42 \pm 3 \mu\text{as}$) are reported by the EHT, respectively.

3 KS black hole with gas at rest

Now, we are going to study the optical appearance of KS black hole surrounded by spherical accretion flow, which is assumed to be optically thin. We consider two cases of accretion: a static spherical accretion model and an infalling spherical accretion.

First, we discuss the shadow image and photon sphere in the background of KS black hole surrounded by static spherical accretion flow. By integrating specific emissivity along the photon path γ , one can obtain the observed intensity of photons for a distant observer as follows [80]–[81]

$$I(\nu_o) = \int_{\gamma} g^3 j(\nu_e) dl_p, \quad (21)$$

where $g \equiv \frac{\nu_o}{\nu_e}$ is gravity redshift factor, ν_e is the radiated photon frequency, $j(\nu_e)$ is the emissivity per unit volume in the rest frame of the emitter, and dl_p is the infinitesimal proper length. For spherically symmetric space-time (5) the redshift factor is $g = f(r)^{1/2}$. By considering monochromatic emission with rest-frame frequency ν_s and the emission radial profile as $1/r^2$ [81], the specific emissivity is given by

$$j(\nu_e) \propto \frac{\delta(\nu_e - \nu_s)}{r^2}. \quad (22)$$

Also, the proper length measured in the rest frame of the emitter for the KS black hole is

$$dl_p = \sqrt{\frac{1}{f(r)} dr^2 + r^2 d\varphi^2} = \sqrt{\frac{1}{f(r)} + r^2 \left(\frac{d\varphi}{dr}\right)^2} dr. \quad (23)$$

Then, using equations (21)–(23) and equation (14), the photon intensity observed by a distant observer can be expressed as

$$I(\nu_o) = \int_{\gamma} \frac{f(r)}{r^2} \sqrt{1 + \frac{b^2 f(r)}{r^2 - b^2 f(r)}} dr. \quad (24)$$

By substituting $f(r)$ from equation (8), the specific intensity of KS black hole shadow and photon rings can be calculated. The observed specific intensity I_o is a function of both the impact parameter b and the Hořava parameter ω . We plot the behavior of intensity as a function of impact parameter for different values of ω in the left panel of Fig. 4. As the figure shows, by increasing the Hořava parameter ω the light intensity of the shadow increases too. According to the figure the observed light intensity sharply increases with the increase of impact parameter and reaches its maximum value at b_{ph} , due to the fact that the light rays round the black

hole several times on the photon sphere, then the light intensity gradually decreases and takes its minimum value.

Furthermore, the KS black hole shadow cast in the (x, y) plane for the static spherical accretion is plotted in the Fig. 5. In each panel, the central disk with a faint of luminosity is the black hole shadow and the brightest ring around the shadow shows the photon ring. As can be seen, with the increase of the parameter ω , the radius of the shadow decreases with a smaller photon ring which is in agreement with Table. 1. Also, according to the figure, by increasing ω the specific intensity increase since, with the increase of ω the strength of gravitational field of KS black hole decreases which leads to lower light rays being trapped by KS black hole and thus in this region higher luminosity of shadow and photon rings being observed. We also conclude that only the KS black holes with larger values of ω have significant deviation from the Schwarzschild black hole with $\omega = 0$ in GR.

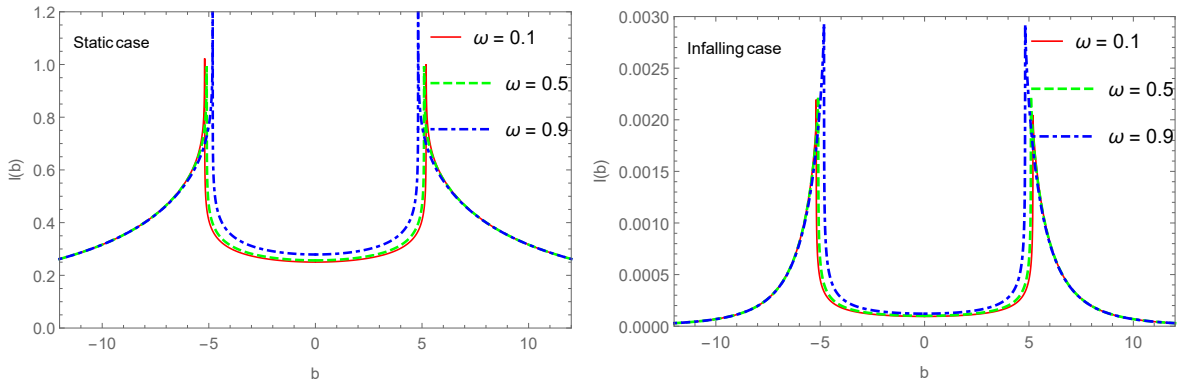


Figure 4: The intensity profile as a function of impact parameter for KS black hole with gas at rest (left panel) and with radially infalling gas (right panel) for different values of ω and $M = 1$.

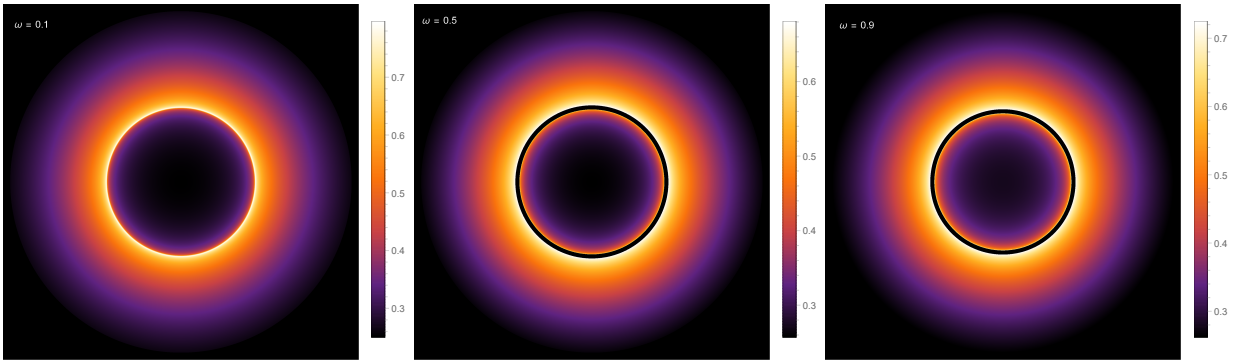


Figure 5: The shadows and photon rings for KS black hole with gas at rest with different values of ω and $M = 1$.

4 KS black hole with infalling gas

In this section we consider the KS black hole surrounded by radial infalling spherical accretion flow. This model is more realistic than the static accretion model since most of accretions are moving in our universe. In this scenario, the redshift factor is related to the velocity of accretion flow as

$$g = \frac{k_\alpha u_o^\alpha}{k_\beta u_e^\beta}, \quad (25)$$

where k_μ is the photon four-velocity, $u_o^\mu = (1, 0, 0, 0)$ is the distant observer four-velocity, and u_e^μ is the four-velocity of the infalling spherical accretion flow. Based on equations (10)-(12), we know that $k_t = 1/b$ is a

constant and k_r can be obtained by the equation $k_\mu k^\mu = 0$. Therefore,

$$\frac{k_r}{k_t} = \pm \sqrt{\frac{1}{f(r)} \left(\frac{1}{f(r)} - \frac{b^2}{r^2} \right)}, \quad (26)$$

where the sign + (-) corresponds to the case that the photon approaches (away from) the black hole. Also, the four-velocity of the infalling accretion is given by

$$\begin{aligned} u_e^t &= \frac{1}{f(r)}, \\ u_e^r &= -\sqrt{1 - f(r)}, \\ u_e^\theta &= u_e^\varphi = 0. \end{aligned} \quad (27)$$

Thus, the redshift factor in equation (25) can be obtained as

$$g = \frac{1}{u_e^t + \left(\frac{k_r}{k_t} \right) u_e^r}. \quad (28)$$

In addition, the proper length is

$$dl_p = k_\alpha u_e^\alpha ds = \frac{k_t}{g |k_r|} dr, \quad (29)$$

where s is the affine parameter along the photon path. Assuming that the specific emissivity has the same form as equation (22), the specific intensity $I(\nu_o)$ in the case of infalling spherical accretion can be expressed as

$$I(\nu_o) \propto \int \frac{g^3 k_t dr}{r^2 |k_r|}. \quad (30)$$

Similar to the static model, the observed intensity for the infalling spherical accretion as a function of impact parameter is plotted in the right panel of Fig. 4. As can be seen, the maximum value of intensity is at b_{ph} but the peak of intensity for infalling case is smaller than the static one. The numerical results of intensity shows that the observed intensity increases with increasing ω . We also present the two-dimensional plot of shadow cast in Fig. 6, showing that the radius of shadow and photon ring decreases with increase of parameter ω , while the shadow and photon rings luminosities increase. Comparing Fig. 5 for the static case with Fig. 6 for the infalling model shows that the shadow region for the infalling accretion flow is darker than that of the static case which is caused by the Doppler effect. Note that the observed shadow size depend only on the space-time geometry, while the luminosities of both the shadow and photon rings are also affected by the accretion flow property.

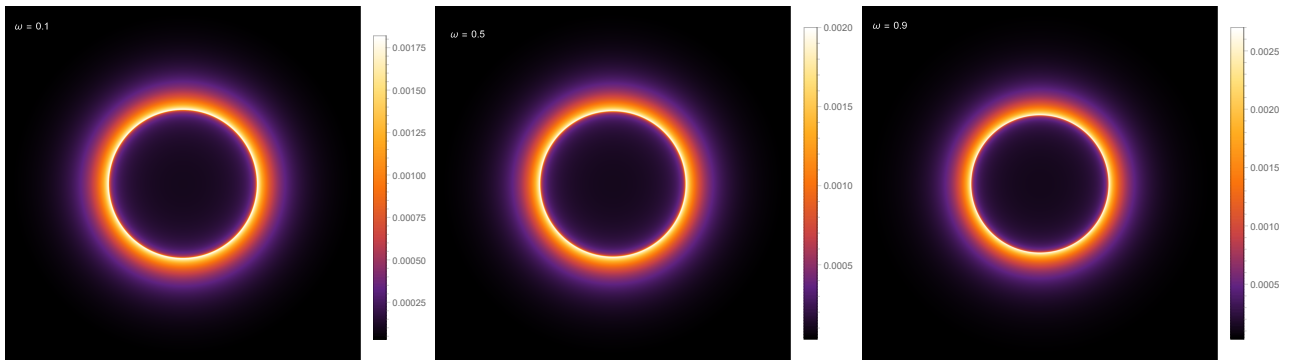


Figure 6: The shadows and photon rings for KS black hole with radially infalling gas with different values of ω and $M = 1$.

5 Conclusions

In this paper, we studied the optical appearance of the KS black holes surrounded by spherical accretion flow. First, we obtained the size of the event horizon radius, the black hole shadow and photon sphere for different values of Hořava parameter ω , and found that the larger the ω parameter is, the smaller the radius of the event horizon, photon sphere and shadow will be. We also obtain the constraint on the parameter ω using the observed shadow diameters measured by the EHT, which is $0 < \omega < 0.7766$ for Sgr A*. However, it is found that the present observational data of M87* can not constrain the KS geometry. Then, we study the observed intensity and the luminosity of KS black hole shadows and photon rings by assuming that the black hole surrounded by static/infalling spherical accretion flow. For both scenarios, we found that the luminosities of the shadow and photon rings of KS black holes increase with the increase of Hořava parameter. This is because by increasing ω , the impact parameter decreases which means that the photons gain more kinetic energy and thus not easily captured by KS black hole which leads to increase the luminosity. Moreover, the results showed that in the case of infalling spherical accretion flow the shadow region is darker than that of the static spherical accretion scenario due to the Doppler effect of the infalling matter.

Acknowledgments

The work of Mohaddese Heydari-Fard is supported by the Iran National Science Foundation (INSF) and the Research Council of Shahid Beheshti University under research project No. 4016024.

References

- [1] K. Akiyama et al, *Astrophys. J* **875** (2019) L1.
- [2] K. Akiyama et al, *Astrophys. J* **875** (2019) L2.
- [3] K. Akiyama et al, *Astrophys. J* **875** (2019) L3.
- [4] K. Akiyama et al, *Astrophys. J* **875** (2019) L4.
- [5] K. Akiyama et al, *Astrophys. J* **875** (2019) L5.
- [6] K. Akiyama et al, *Astrophys. J* **875** (2019) L6.
- [7] K. Akiyama, A. Alberdi, W. Alef, J. C. Algaba and R. Anantua, *Astrophys. J. Lett* **930** (2022) L12.
- [8] J. L. Synge, *Mon. Not. R. Astron. Soc* **131** (1966) 463.
- [9] J. M. Bardeen, in *Black holes*, Proceeding of the Les Houches Summer School, Session 215239, edited by C. De Witt and B.S. De Witt (Gordon and Breach, NewYork, 1973).
- [10] P. V.P. Cunha, C. A. R. Herdeiro, B. Kleihaus, J. Kunz and E. Radu, *Phys. Lett. B* **768** (2017) 373.
- [11] S. Vagnozzi and L. Visinelli, *Phys. Rev. D* **100** (2019) 024020.
- [12] S. V. M. C. B. Xavier, P. V. P. Cunha, L. C. B. Crispino and C. A. R. Herdeiro, *Int. J. Mod. Phys. D* **29** (2020) 2041005.
- [13] A. Narang, S. Mohanty and A. Kumar, arXiv:2002.12786 [gr-qc].
- [14] M. Khodadi and G. Lambiase, *Phys. Rev. D* **106** (2021) 104050.
- [15] J. A. V. Campos, M. A. Anacleto, F. A. Brito and E. Passos, *Sci. Rep* **12** (2022) 8516.
- [16] M. Heydari-Fard, M. Heydari-Fard and H. R. Sepangi, *Phys. Rev. D* **105** (2022) 124009.

- [17] M. Heydari-Fard and M. Heydari-Fard, *Int. J. Mod. Phys. D* **31** (2022) 2250066.
- [18] M. Jusufi, M. Azreg-Ainou, M. Jamil and E. N. Saridakis, *Universe* **8** (2022) 102.
- [19] S. Vagnozzi, R. Roy and Y. D. Tsai, et al., arXiv:2205.07787 [gr-qc].
- [20] A. Belhaj and Y. Sekhmani, *Gen. Rel. Grav* **54** (2022) 17.
- [21] J. Badia and E. F. Eiroa, *Phys. Rev. D* **107** (2023) 124028.
- [22] J. P. Luminet, *Astron. Astrophys* **75** (1979) 228.
- [23] H. Falcke, F. Melia and E. Agol, *Astrophys. J. Lett* **528** (2000) L13.
- [24] P. V. P. Cunha, N. A. Eirco, C. A. R. Herderio and J. P. S. Lemos, *JCAP* **03** (2020) 035.
- [25] S. E. Gralla, D. E. Holz and R. M. Wald, *Phys. Rev. D* **100** (2019) 024018.
- [26] R. Narayan, M. D. Johnson and C. F. Gammie, *Astrophys. J. Lett* **885** (2019) L33.
- [27] X. X. Zeng, H. Q. Zhang and H. Zhang, *Eur. Phys. J. C* **80** (2020) 872.
- [28] X. X. Zeng and H. Q. Zhang, *Eur. Phys. J. C* **80** (2020) 1058.
- [29] S. Guo, K. J. He, G. R. Li and G. P. Li, *Class. Quant. Grav* **38** (2021) 165013.
- [30] X. Qin, S. Chen and J. Jing, *Class. Quant. Grav* **38** (2021) 115008.
- [31] K. Saurabh and K. Jusufi, *Eur. Phys. J. C* **81** (2021) 490.
- [32] Q. Gan, P. Wang, H. Wu and H. Yang, *Phys. Rev. D* **104** (2021) 044049.
- [33] H. M. Wang, Z. C. Lin and S. W. Wei, *Nucl. Phys. B* **985** (2022) 116026.
- [34] S. Guo, G. R. Li and E. W. Liang, *Phys. Rev. D* **105** (2022) 023024.
- [35] X. X. Zeng, K. J. He and G. P. Li, *Sci. China Phys. Mech. Astron.* **65** (2022) 290411.
- [36] K. J. He, S. Guo, S. C. Tan and G. P. Li, *Chin. Phys. C* **46** (2022) 085106.
- [37] M. Okyay and A. Övgün, *JCAP* **01** (2022) 009.
- [38] S. Hu, C. Deng, D. Li, X. Wu and E. Liang, *Eur. Phys. J. C* **82** (2022) 885.
- [39] S. Guo, G. R. Li and E. W. Liang, *Class. Quant. Grav* **39** (2022) 135004.
- [40] X. X. Zeng, K. J. He, G. P. Li, E. W. Liang and S. Guo, *Eur. Phys. J. C* **82** (2022) 764.
- [41] Y. X. Chen, P. H. Mou and G. P. Li, *Symmetry* **14** (2022) 1959.
- [42] M. Heydari-Fard, arXiv:2209.09103 [gr-qc].
- [43] S. J. Ma, T. C. Ma, J. B. Deng and X. R. Hu, arXiv:2206.12820 [gr-qc].
- [44] X. X. Zeng, M. I. Aslam and R. Saleem, *Eur. Phys. J. C* **83** (2023) 129.
- [45] A. Uniyal, R. C. Pantig and A. Övgün, *Phys. Dark. Univ* **40** (2023) 101178.
- [46] X. J. Wang, X. M. Kuang, Y. Meng, B. Wang and J. P. Wu, *Phys. Rev. D* **107** (2023) 124052.
- [47] S. Wen, W. Hong and J. Tao, *Eur. Phys. J. C* **83** (2023) 277.
- [48] H. Lü , J. Mei, and C. N. Pope, *Phys. Rev. Lett* **103** (2009) 091301.

- [49] A. Kehagias and K. Sfetsos, *Phys. Lett. B* **678** (2009) 123.
- [50] A. N. Aliev and Ç. Şentürk, *Phys. Rev. D* **82** (2010) 104016.
- [51] H. W. Lee, Y.W. Kim, and Y. S. Myung, *Eur. Phys. J. C* **70** (2010) 367.
- [52] T. Harko, Z. Kovács and F. S. N. Lobo, *Phys. Rev. D* **80** (2009) 044021.
- [53] R. A. Konoplya, *Phys. Lett. B* **679** (2009) 503
- [54] T. Harko, Z. Kovács and F. S. N. Lobo, *Class. Quant. Grav* **28** (2011) 165001.
- [55] Z. Horváth, L. A. Gergely, Z. Keresztes, T. Harko and F. S. N. Lobo, *Phys. Rev. D* **84** (2011) 083006.
- [56] T. Harko, Z. Kovács and F. S. N. Lobo, *Proc. Roy. Soc. Lond. A* **467** (2011) 1390.
- [57] F. Atamurotov, A. Abdujabbarov and B. Ahmedov, *Astrophys. Space Sci* **348** (2013) 179.
- [58] R. S. S. Vieira, J. Schee, W. Kluźniak, Z. Stuchlík and M. Abramowicz, *Phys. Rev. D* **90** (2013) 024035.
- [59] Z. Stuchlík, J. Schee A. Abdujabbarov, *Phys. Rev. D* **89** (2014) 104048.
- [60] Z. Stuchlík and J. Schee, *Class. Quant. Grav* **31** (2014) 195013.
- [61] S. Hensh, A. Abdujabbarov, J. Schee and Z. Stuchlík, *Eur. Phys. J. C* **79** (2019) 533.
- [62] S. Hensh, J. Schee, A. Abdujabbarov and Z. Stuchlík, *Eur. Phys. J. Plus* **137** (2022) 242.
- [63] M. Alloqulov, F. Atamurotov, A. Abdujabbarov and B. Ahmedov, *Chin. Phys. C* (2023).
- [64] M. i. Park, *JHEP* **09** (2009) 123.
- [65] E. Kiritsis and G. Kofinas, *Nucl. Phys. B* **821** (2009) 467.
- [66] G. Calcagni, *JHEP* **09** (2009) 112.
- [67] R. Brandenberger, *Phys. Rev. D* **80** (2009) 043516.
- [68] A.Wang and Y.Wu, *JCAP* **07** (2009) 012.
- [69] S. Mukohyama, *JCAP* **06** (2009) 001.
- [70] S. Dutta and E. N. Saridakis, *JCAP* **01** (2010) 013.
- [71] M. Jamil and E. N. Saridakis, *JCAP* **07** (2010) 028.
- [72] M Heydari-Fard, *Gen. Rel. Grav* **42** (2010) 2729.
- [73] M. Jamil, E. N. Saridakis and M. R. Setare, *JCAP* **11** (2010) 032.
- [74] F. Kheyri, M. Khodadi and H. R. Sepangi, *Eur. Phys. J. C* **73** (2013) 2286.
- [75] F. Kheyri, M. Khodadi and H. R. Sepangi, *Annals Phys.* **332** (2013) 75.
- [76] N. A. Nilsson and E. Czuchry, *Phys. Dark. Univ* **23** (2019) 100253.
- [77] G. P. Li and K. J. He, *JCAP* **06** (2021) 037.
- [78] C. M. Claudel, K. S. Virbhadra and G. F. R. Ellis, *J. Math. Phys* **42** (2001) 818.
- [79] V. Perlick and O.Y. Tsupko, *Phys. Rep* **947** (2022) 1.
- [80] M. Jaroszynski and A. Kurpiewski, *Astron. Astrophys* **326** (1997) 419.
- [81] C. Bambi, *Phys. Rev. D* **87** (2013) 107501.